THE ROYAL SOCIETY

Measuring bubble nucleation temperature on the surface of a rapidly heated thermal ink-jet heater immersed in a pool of water

By C. T. Avedisian[1], W. S. Osborne[1]†, F. D. McLeod[2] and C. M. Curley[2]‡

[1]*Sibley School of Mechanical and Aerospace Engineering,* [2]*School of Electrical Engineering, Cornell University, Ithaca, New York, NY 14853-7501, USA*

Received 29 July 1998; revised 18 December 1998; accepted 20 January 1999

We describe a method for measuring the average surface temperature of a small square thin metallic film deposited on a silicon substrate and immersed in subcooled water during a voltage pulse of short duration. The thin film studied is a material used in the current generation of commercial 'desk-jet' printers and comprises a mixture of tantalum and aluminium 65 μm wide and 0.2 μm thick. The experiment uses a bridge circuit with a dynamic amplifier design to measure the evolution of electrical resistance, coupled with a separate calibration of the thin film resistor element with temperature to determine average surface temperature. Voltage pulses of 5 μs typical duration are applied to the thin films. An 'inflection' point in the resulting evolution of heater surface temperature identifies bubble nucleation.

The calibration of the heater resistance with temperature showed a hysteresis effect that required a burn-in process to stabilize the electrical resistance. With the calibration curve obtained, resistance was converted to temperature and the results analysed. For low power input the average surface temperature exhibited an oscillatory behaviour which indicated a cyclic growth/collapse process often found in nucleate boiling. At higher powers, the oscillatory behaviour disappeared and gave way to an exponential variation of temperature with time similar to a lumped capacitance behaviour of a thermal system. An inflection point in the evolution of surface temperature was found that signified bubble nucleation. The largest heating rate and highest nucleation temperature measured were 0.25×10^9 °C s^{-1} and 556 K, respectively. This temperature is in good agreement with homogeneous nucleation theory as applied to a surface. The contact angles needed for measured nucleation temperatures to agree with predictions are within the range that is typical for water on metallic surfaces.

Keywords: ink jet; bubble jet; heat transfer; metastable liquid; homogeneous nucleation; thin films

† Permanent address: Vancouver Printer Operation, Hewlett–Packard Co., Vancouver, Wa., Canada 98668-8906.

‡ Permanent address: Innotek, 120 Brook Way, Ithaca, New York, NY 14850, USA.

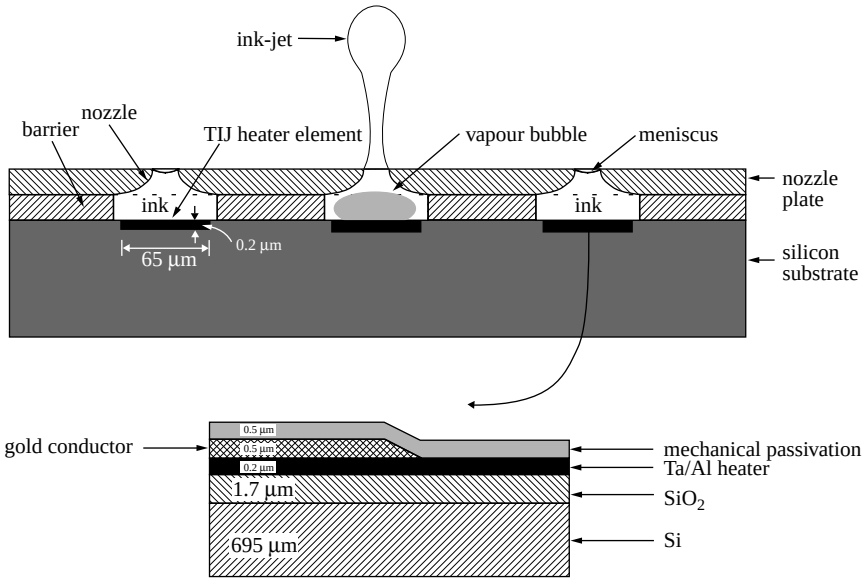

Figure 1. Illustration of the droplet ejection process by bubble nucleation at a surface (not to scale). Mechanical passivation was not placed on heaters studied here. The active area for boiling is the exposed region beyond the gold conductor.

1. Introduction

A method for producing hardcopy documentation that continues to grow in popularity is ink-jet printing. It involves creating liquid droplets from a nozzle by a piston effect produced by bubble nucleation at a rapidly heated thin metallic film (Nielsen 1985). The bubble pressurizes the surrounding ink to force liquid through an orifice to create a droplet which then impacts the print media. Programmed delivery of droplets creates the print characters. Figure 1 is a schematic of the droplet ejection process. Details of the layered thin film heater are also shown.

It has been speculated from the earliest days of development of the ink-jet printer that the ink must be superheated before bubble nucleation occurs. But precisely how large the superheat needed to be for acceptable print quality, and actually was in the commercial product, has so far been uncertain. The upper limit is homogeneous nucleation and the lower limit is the normal boiling point. For inks which are water-based, the corresponding 200 K range produces considerable uncertainty in the physics of the process. It was first hypothesized by Allen *et al.* (1985) that homogeneous nucleation is the preferred mechanism because of its independence on heater surface condition. Heterogeneous nucleation arises from pre-existing vapour nuclei trapped in surface imperfections when the surface is flooded with liquid. The many bubbles and piston-like effects in the liquid that result from this form of bubble nucleation lead to unstable droplet ejection and poor print quality. The variable for identifying the physics of the nucleation process is the heater surface temperature.

In this paper we describe an experimental arrangement for measuring accurately the average surface temperature of a single heater element used in commercial desk-jet or 'thermal ink-jet' (TIJ) printers. The results presented also have a more general interest for studying bubble nucleation of highly superheated liquids. The dynamic

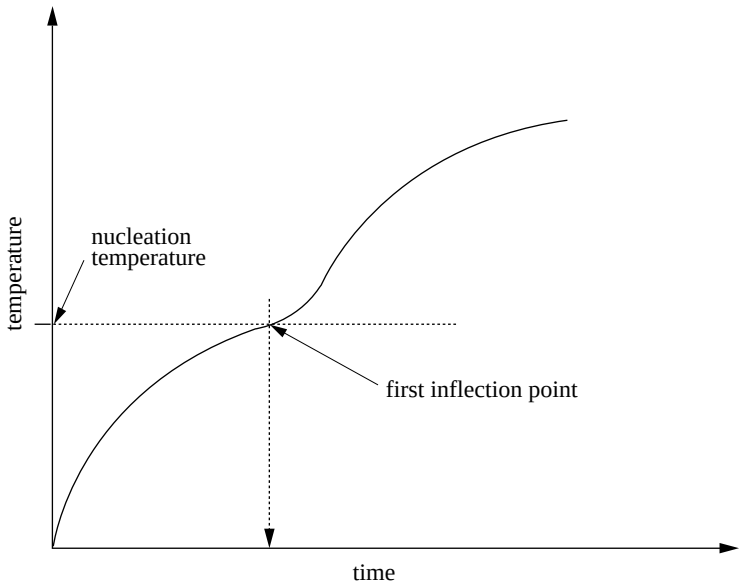

Figure 2. Schematic of surface temperature change showing influence of bubble nucleation.

conditions experienced by the heaters in operation are reproduced in our experiments, and these conditions create considerable challenges for measurements.

In commercial printers, the print heads are fired at high frequencies and short durations that are less than 5 μs long. The heater is a small square thin film in the design studied in this paper, 64.5 μm wide, 0.2 μm thick and placed onto a silicon substrate 695 μm thick. Figure 1 shows the structure. A mechanical passivation layer is used in the commercial product to protect the resistance heater from the bubble collapse process. The passivation layer electrically isolates the heater material from thin film thermocouples that may be placed on it, such as those used by Olive *et al*. (1988) and Lee & Tirumala (1988). And it adds a thermal resistance between the heater and liquid, which increases the response time of the surface to changes in surface temperature associated with the thermal shock that accompanies rapid bubble nucleation. Detecting this temperature change is at the heart of measuring the incipient nucleation temperature as described below. Heaters were used without a mechanical passivation layer in the present study.

The incipient nucleation temperature is identified by a change in the heating rate of the surface due to the transition from liquid–solid to vapour–solid contact because of the formation of the bubble. Figure 2 shows a schematic of the effect that results from this transition we desire to capture by measuring the evolution of average surface temperature during pulse heating. The early transient of a TIJ heater in figure 2 is characterized by an almost exponential variation of temperature with time because of the small size of the heater that makes valid a lumped capacitance approximation in view of the small Biot number. When a bubble forms, an inflection point appears in the evolution of surface temperature which must be resolved for accurate measurement of temperature.

Prior studies on pulse heating liquids using resistance heating of various geometries —wires and plates—have used the variation of material resistance with temperature

to achieve a dual purpose of the heater: as a heat source to affect a phase change in the liquid and as a temperature sensor through the material's variation of electrical resistivity with temperature. The ability to detect the incipient nucleation temperature is dependent on fluid and solid properties: larger differences between vapour and liquid thermal conductivity and strong variations of electrical resistivity with temperature will produce a sharper effect. The studies by Skripov (1974), Okuyama *et al*. (1988), Okuyama & Iida (1990) and Derewnicki (1985) for fine diameter platinum wires, and by Iida *et al*. (1993, 1994) for thin film platinum plates, based measurement of the incipient nucleation temperature on the evolution of surface temperature (like in figure 2), obtained by measuring the resistance during the input power pulse. Platinum is a good choice for serving as both a thermistor and heat source because of its strong variation of electrical resistivity with temperature compared with other metals. However, the metal of a TIJ heater is a proprietary blend of materials that include the metals aluminium (Al) and tantalum (Ta). This alloy was found in our study to have a much weaker dependence of temperature on resistivity. This fact makes it more difficult to use the metal's change in resistance with temperature as a sensor, yet we have to use the actual printer material in a nucleation study because of the unique wetting characteristics that effect the nucleation temperature. A material like platinum is irrelevant to simulating printer conditions.

Figure 3 compares the variation of electrical resistivity of platinum (Lide 1992) with a TIJ thin film material (as measured from the instrumentation discussed in this paper). The variations are in opposite directions, but moreover the change in resistivity of the TIJ material is much smaller than for platinum. To measure heater surface temperature to an accuracy of $\pm 0.5\ ^{\circ}\mathrm{C}$ for the TIJ print head requires the ability to resolve $0.016\ \Omega$ on a base value of *ca.* $15\ \Omega$ at a frequency of 200 kHz over a $5\ \mu\mathrm{s}$ time period, which is the typical duration of a TIJ print operation. Sensitive circuitry is needed to amplify the small change in resistance without introducing significant noise that would compromise the accuracy of the measurement. This problem is evident in the study by Poppel (1989), who reported surface temperature measurements of TIJ heaters, but few details are provided.

In the following, we give details of an experimental arrangement for measuring average surface temperature of a TIJ print head during pulse heating while the heater is submerged in a pool of water. Water is used as the test fluid because commercial inks are water based. The water is at room temperature far from the heated surface. We discuss two major parts of the instrumentation: (i) the electrical circuitry required to measure resistance during a voltage pulse; and (ii) calibration of the resistor with temperature to convert measured resistances to average surface temperature. Then, we present results of experiments to measure the incipient nucleation temperature of water for a range of input powers and heat fluxes, and compare the measurements with models for homogeneous bubble nucleation.

2. Experiment

(*a*) *Heater elements*

Thin film heaters were manufactured for this study by the Hewlett–Packard Corporation. They were provided on a single Si wafer $69\ \mu\mathrm{m}$ thick and 150 mm in diameter. Each wafer contains 353 'chips' that contain the metallization of the heater elements. Figure 4 is a photograph of a single wafer sitting on a table (view is from an angle)

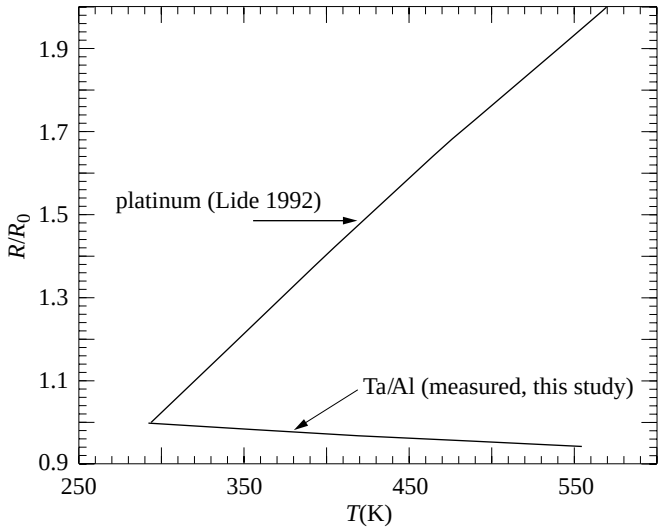

Figure 3. Dependence of resistivity on temperature for platinum (data from Lide 1992) and a tantalum–aluminium alloy of an ink-jet thin film as measured in this study.

which shows the 353 chips. Each of the chips is 3.5 mm wide and 7.5 mm long and contains 50 square heater elements which are 64.5 μm wide. Figure 5 is a photomicrograph of one individual chip that has been singulated from a 150 mm Si wafer. The chips are fabricated without a passivation layer, to enhance the sensitivity of the surface to detect phase change in the liquid in contact with it. A thin SiO_2 layer, *ca.* 1.6 μm thick, is placed on the Si substrate prior to depositing the resistor material. This layer serves as a thermal barrier to reduce rapid heat removal into the Si substrate. The serpentine arrays on the right and left sides in the middle of the figure (between the '+' signs) are calibration resistors made of the same material as the heater element.

The heater elements themselves—50 are included on each chip—are at the ends of the gold (bright) circuit lines and are barely visible in figure 5 as the darker small rectangles just above and below the bar that runs across the centre of the photo. The heaters are 0.2 μm thick and composed of a proprietary mixture of tantalum and aluminium. The circuit lines leading up to the heater elements are gold traces visible as the bright lines in figure 5. They run over identical Ta–Al patterns except at the ends, where bare Ta–Al is exposed. The 'black' zones in figure 5 are the exposed Si substrate. Individual heater elements are visible in figure 5 as the darker small squares at the ends of the brighter gold traces. The dominant electrical path is the gold overlays up to the exposed ends. Figure 6 shows one individual heater element (50 of these heaters are on in figure 4). The heater element is a square 64.5 μm wide. The bright areas on the top and bottom of figure 6 show the gold overlays; the dark areas to the side are exposed Si.

Single test chips were cut from the Si wafer and glued into the base of a flat pack. Electrical connections were made to the edge of the flat pack from the ends of the gold leads of the test chip by wire bonding. A single test chip was flooded with water which covered all 50 resistors, though only one was used at a time.

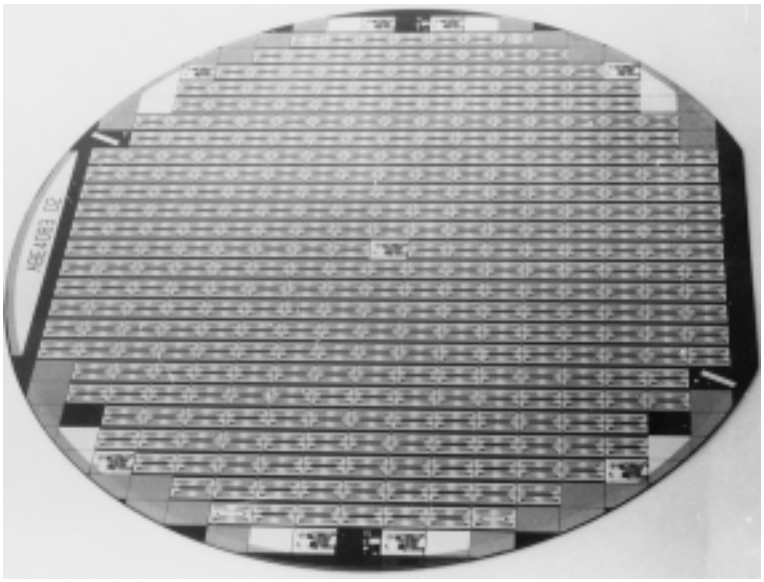

Figure 4. Photograph of a 150 mm diameter silicon wafer that contains 353 individual chips.

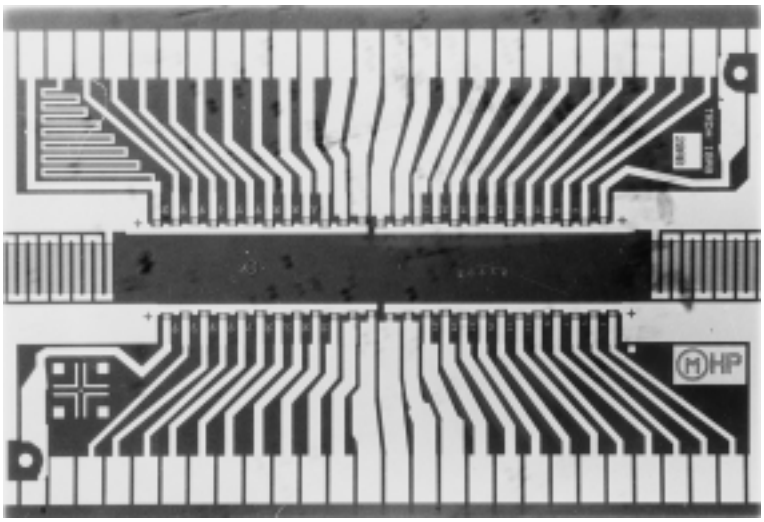

Figure 5. Photomicrograph of a single chip (see figure 4) that was singulated from a 150 mm diameter Si wafer. An individual TIJ heater element is shown as the tiny grey squares at the ends of bright (gold) traces. Portions of two calibration resistors are seen between the '+' marks on the right and left side.

(*b*) *Bridge and amplifier circuit*

The detection methodology used for measuring average heater surface temperature of the TIJ print head is based on measuring the average TIJ *resistance* during application of a square voltage pulse. A separate calibration of TIJ resistance with temperature yields the average surface temperature. The goal of the instrumentation design is to measure the evolution of TIJ resistance due to a square wave voltage

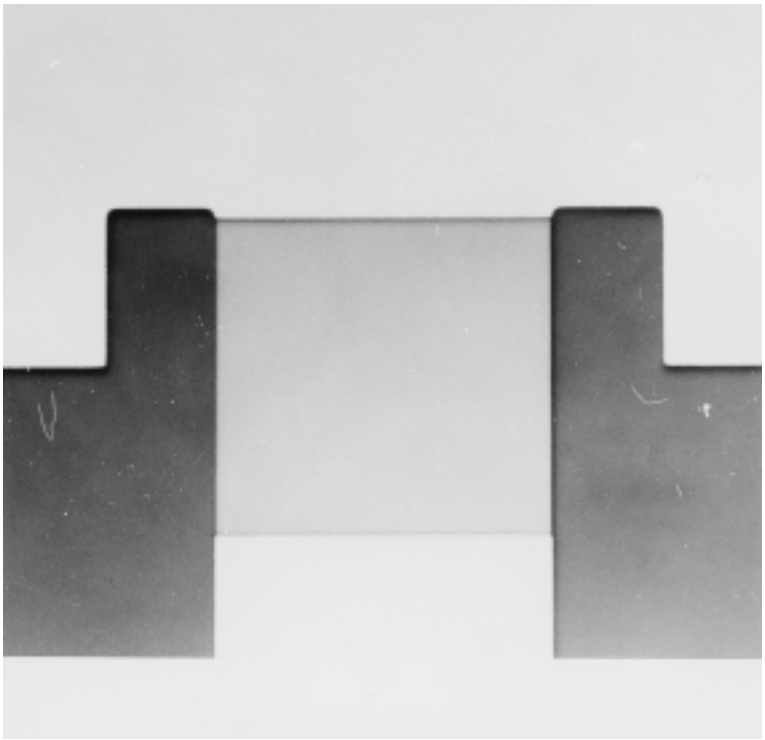

Figure 6. Photomicrograph of a single thin film TIJ heater element (square region) composed of a Ta–Al alloy. The lightest regions are gold. The dark areas are exposed Si. The square is a 64.5 μm wide TIJ heater element.

pulse of about 5 μs duration. We describe here the basic circuitry for this resistance measurement.

The circuitry consists of two parts: (i) a bridge circuit with the TIJ resistor placed in one leg; and (ii) an amplifier circuit that monitors only the *change* in resistance during a firing pulse from room temperature. This latter feature is necessary because of the expected small change in resistance of the TIJ material during the heating phase. Figure 7 is a schematic that shows the bridge and amplifier circuit. The thin film heater element is in the A–D branch of the bridge and is labelled $R_{1\mathrm{h}}$. V_{ref} is the input voltage, $R_{1\mathrm{t}}$ is a 'trace' resistance that is separated from $R_{1\mathrm{h}}$ to account for the connections to the TIJ resistor of all the leads and gold traces to $R_{1\mathrm{h}}$, and R_6 is a potentiometer for balancing the bridge. $R_{1\mathrm{t}}$ was measured with micro-manipulator probes that could be positioned right up to the edge of a 64.5 μm square TIJ ($R_{1\mathrm{h}}$) element. With this instrumentation we measured $R_{1\mathrm{t}} \approx 6.864\,\Omega$.

The bridge is stimulated by V_{ref} using a HP 214B pulse generator that controls the pulse duration. The output of the pulse generator controls the MOSFET driver (IRF530) which excites the bridge. The pulse magnitude was set by an HP 6115A precision power supply. Input power was provided either as a single pulse or operated at a preset frequency. In the latter mode, visual inspection of the voltage traces on the oscilloscope confirmed the high degree of repeatability of the voltage output from the TIJ leg of the bridge circuit. The pot R_6 is used to balance the bridge at ambient temperature such that the bridge output nodes B and D produce equal

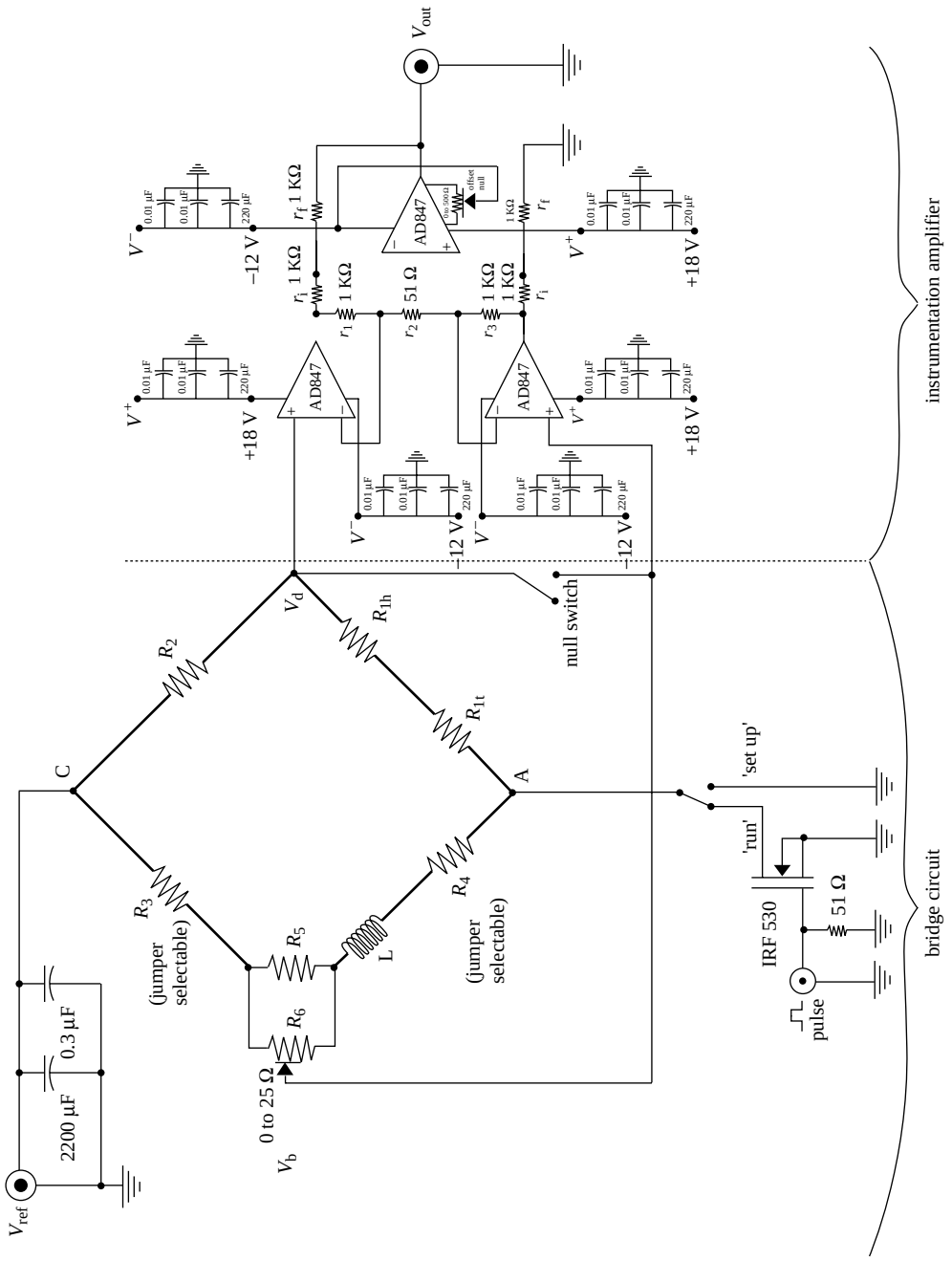

Figure 7. Schematic of bridge circuit showing the instrumentation amplifier.

voltages, $V_b = V_d$. During operation, $V_d - V_b \approx 40$ mV. Because of the comparatively large magnitude of V_{ref}, of the order of volts, a differential amplifier was constructed to record only the change in this voltage difference.

The amplifier section in figure 7 is based upon two buffer amplifiers in a differen-

tial configuration, which feed a third output stage. The bridge 'unbalance' voltage, $V_\mathrm{d} - V_\mathrm{b}$, is amplified by a X210 broad-band high slew rate instrumentation amplifier. A large $\frac{1}{3}V_\mathrm{ref}$ common voltage step at the start and end of a test pulse is rejected by the high common mode rejection ratio (greater than 86 dB) of the instrumentation amplifier configuration. The AD874 operational amplifiers used in this design have a bandwidth of 50 MHz, unity gain bandwidth and a slew rate of 225 V $\mu\mathrm{s}^{-1}$.

Given that V_ref is the known input voltage to the bridge, R_1h is obtained as follows. Let

$$\Delta V_\mathrm{bridge} = V_\mathrm{b} - V_\mathrm{d}, \tag{2.1}$$

$$R_1 = R_\mathrm{1h} + R_\mathrm{1t} \tag{2.2}$$

and

$$V_\mathrm{out} = A\Delta V_\mathrm{bridge}, \tag{2.3}$$

where A is the amplifier gain (i.e. $A = (r_1 + r_2 + r_3)/r_2(r_\mathrm{f}/r_\mathrm{i})$) and lower case '$r$' signifies resistors in the amplifier circuit). From the relationship between voltage and resistance,

$$V_\mathrm{d} = \frac{R_1}{R_1 + R_2}V_\mathrm{ref}. \tag{2.4}$$

If the bridge is initially unbalanced, its offset can be compensated. The initial value of V_out is

$$V_\mathrm{out} = \frac{1}{A}\left(V_\mathrm{ref}\frac{V_\mathrm{offset}}{V_\mathrm{test}}\right), \tag{2.5}$$

which gives

$$V_\mathrm{b} = V_\mathrm{ref}\left(\frac{R_1}{R_1 + R_2} + \frac{1}{A}\frac{V_\mathrm{offset}}{V_\mathrm{test}}\right). \tag{2.6}$$

V_b is assumed to be constant relative to changes in V_d. Written in terms of V_out, equation (2.5) becomes

$$V_\mathrm{out} = A\left(V_\mathrm{b} - V_\mathrm{ref}\left(\frac{R_1}{R_1 + R_2}\right)\right) \tag{2.7}$$

or

$$w = \frac{R_1}{R_1 + R_2} = \frac{1}{V_\mathrm{ref}}\left(V_\mathrm{b} - \frac{V_\mathrm{out}}{A}\right). \tag{2.8}$$

Hence

$$R_1 = R_2\left(\frac{w}{1 - w}\right). \tag{2.9}$$

The total input power to R_1h is computed from

$$P = R_\mathrm{1h}\left(\frac{V_\mathrm{d}}{R_\mathrm{1h} + R_\mathrm{1t}}\right)^2. \tag{2.10}$$

The power calculated from equation (2.10) is the *total* power into the TIJ heater. Part of this power is dissipated in the liquid and part is dissipated through the back side of the Si substrate. The latter is estimated using a conduction network consisting of water, SiO_2 and bulk Si thermal resistances all in series. Heat is input to the node representing the TIJ element between the water and SiO_2 layers. The layer thicknesses were $L_w = 4\,\mu m$, $L_{SiO_2} = 1.6\,\mu m$ and $L_{Si} = 100\,\mu m$, where the water and Si layer thicknesses were taken at values where room temperature is realized as determined by a finite element model of transient heat transfer in the network (Osborne 1996). Defining

$$R''_w \equiv \frac{L_w}{k_w}, \qquad R''_{Si} \equiv \frac{L_{Si}}{k_{Si}} \quad \text{and} \quad R''_{SiO_2} \equiv \frac{L_{SiO_2}}{k_{SiO_2}},$$

the total thermal resistance becomes

$$R''_T = R''_w \frac{R''_{Si} + R''_{SiO_2}}{R''_{Si} + R''_{SiO_2} + R''_w}.$$

By using thermal conductivity values from Incropera & DeWitt (1996), we found that *ca.* 64% of the electrical power into the TIJ heater is dissipated through the water and the remainder is dissipated through the solid substrate.

The amplifier output was interfaced with an HP 54111D digital oscilloscope which has a 2 GHz bandwidth. The amplifier output voltage was digitized by the scope with a resolution of 50 points μs^{-1} and stored in one of the two channels of the scope memory. The stored wave form was then transported via an HPIB interface to a Dell 466LE computer with HPIB communications board, HPSICL control language and a custom data acquisition program written in MS Visual Basic.

(*c*) *Considerations*

A considerable problem encountered was an artefact created in the output signal caused by high-frequency cycling and inductive pickup which caused a voltage 'spike' at the beginning ('on') and end ('off') of the switching. This effect arises by differences in the capacitance or inductance of any segment of the bridge that result in a voltage developing during switching, as well as by the large transient current through the heater during operation. Poppel (1989) also observed a similar effect in his pulse heating experiments. The spikes did not significantly affect the location of the 'kink' in figure 2, but it did alter the rise signal form. Therefore, we took efforts to reduce this effect. We found that by adding a small amount of inductance (i.e. 1 μH inductance typical for L in figure 7) to the A–B leg of the bridge as shown in figure 7, this switching artefact was reduced to an acceptable level. An inductor was fabricated by forming a copper wire coil and inserting into it a ferrite cylinder. The cylinder was 4.56 mm in diameter and 9.56 m long. The coil consisted of six turns of 0.81 mm diameter copper wire wound around the core. By turning the ferrite core during high-frequency pulsing, and from real-time observation on the scope screen, the switching noise could be reduced. This tuning operation was a trial adjustment for each V_{ref} value.

3. Calibration of the electrical resistance

The relationship between electrical resistance and temperature is crucial to identifying the nucleation temperature. The challenge in obtaining this relationship is

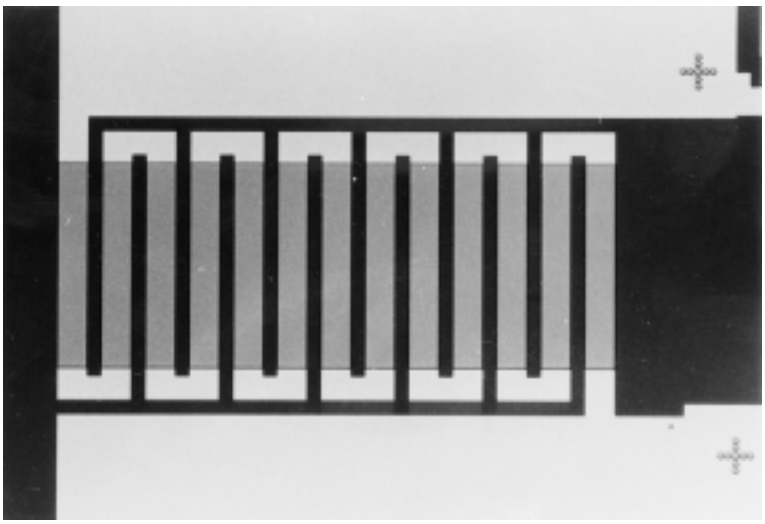

Figure 8. Photomicrograph of a serpentine calibration resistor, composed of identical material and thickness as an individual TIJ heater element (as in shown in figure 6). '+' marks can be referenced to figure 5, which shows part of a calibration resistor on a singulated chip.

that of measuring accurately a small resistance change over the temperature range of interest on a comparatively large base value. Because of this problem we used a larger resistor to amplify the resistance. This larger resistance was fabricated in an identical manner to an individual TIJ heater element. Its width was the same as a TIJ element. The only difference was that it was much longer, to amplify the resistance. The calibration resistor consisted of lines 0.2 μm thick, 64.5 μm wide and 6444.62 μm long coiled in a serpentine network of 495.74 μm long lines. They are partly shown in figure 5 on the right and left edges. Figure 8 is a photomicrograph of a full calibration resistor (the '+' marks in figure 8 can be referenced to figure 5). In the fabrication of these calibration resistors on a chip, gold was placed over the serpentine pattern and etched away over lengths of 495.74 μm to expose the Ta–Al sub-layer. These resistor lengths are visible in figure 8 as the darker vertical lines.

During calibration the resistor is placed in close proximity to a temperature probe (HP2804A quartz thermometer accurate to ±0.075 °C up to 250 °C) inside a computer controllable furnace (Barnstead/Thermolyne 48000 programmable furnace). Resistance was measured (to ±1 μΩ) with a HP3457 multimeter using the four-wire technique. Computer control was effected by a Dell OptiPlex controller with HP, HPIB card, HPSICL command language and a custom MS Visual Basic program for controlling the calibration and downloading the data.

The procedure for calibration consisted of increasing the furnace temperature in controlled steps starting from room temperature, holding the furnace temperature at each step until the temperature and resistivity of the calibration resistor stabilized or a preset time limit (typically six hours) was exceeded. The control software gathers electrical resistance measurements and stores the data to disk. In order to mount the chips for calibration, they are first singulated from the silicon wafers and then wire-bonded to provide electrical connections with the test equipment. A flat pack was used to mount the test chip. The flat pack is soldered to the four-wire measurement system using an Indalloy #165 solder. Figure 9 shows the measured variation of

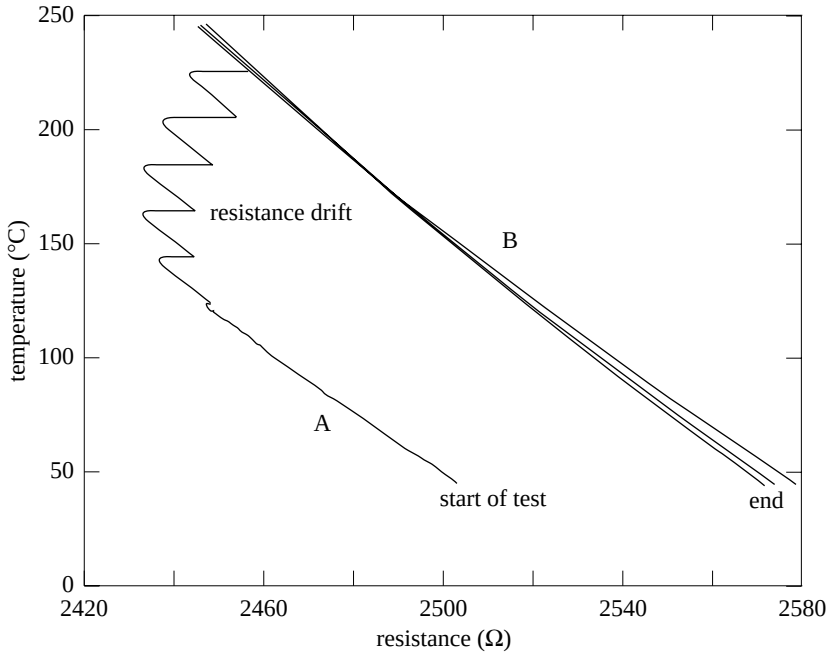

Figure 9. Resistance as a function of temperature for a calibration resistor. Branch 'A' shows the initially unstable resistance and branch 'B' indicates stability after three cycles over the indicated temperature range.

resistance with temperature for five temperature cycles between 40 °C (313 K) and 250 °C (523 K). Three points about the results are the following.

Firstly, the resistance *decreases* as temperature *increases*. This trend is contrary to many pure metals, which exhibit an increase of resistivity as temperature increases. The trend for the TIJ heater material is, however, consistent with semiconductor materials which show a negative coefficient of resistance with temperature. Secondly, the resistance changes *ca.* 1.57 Ω for each degree Celsius increment in temperature. Since the calibration resistance is 100 (or more precisely 99.91) times larger than an individual heater resistance, the change per degree of an individual TIJ heater element is small, *ca.* 0.016 Ω. This fact motivated the bridge and amplifier design discussed previously. Thirdly, the resistance showed a hysteresis effect with temperature: cycling temperature produced trends that fell on different tracts. Pure metals such as Al and Ta do not show this behaviour (e.g. Lide 1992). Only after repeated temperature cycling in the oven did the resistance appear to 'lock' into a unique relationship between temperature and resistance. This effect is shown in figure 9 by the different tracts 'A' and 'B'.

Below 398 K (125 °C) in figure 9, the variation of resistance with temperature is monotonic. Above 125 °C it begins to oscillate, then restabilizes above 227 °C (500 K). Upon cooling to room temperature from 227 °C, the resistance is stable. Clearly, material changes have occurred above 125 °C. Two possibilities are a phase transition and annealing of defects (recovery/recrystallization).

We do not know the precise composition of the Ta–Al thin film heaters studied. But if, for example, they were a mixture of Al and $TaAl_3$, then a phase transition

could occur as temperature is increased, whereby $TaAl_3$ decomposes and the Ta molecules become dispersed throughout a matrix of Al molecules. The accompanying change in crystallographic structure can produce a change of electrical resistivity. More importantly, as phase transitions are typically reversible while the variation of resistivity with temperature displayed in figure 9 shows hysteresis as temperature is varied, we do not believe that the thin film metal is experiencing a phase transition during calibration.

In annealing, defect- and strain-free regions form and grow as temperature increases until the strained regions are eliminated and the entire material recrystallizes. The electrical resistivity will change as the material recrystallizes and there could be a dopant in the thin film that decreases the recrystallization temperature of the Ta–Al mixture to initiate this change at a low temperature. Once recrystallization occurs it is generally irreversible, so that the electrical resistance would therefore be uniquely defined by temperature. The change in the calibration curve in figure 9 from 'A' to 'B' shows this effect and thus of the metal being annealed during the calibration procedure. A related observation is that, even for heaters that did not go through temperature cycling like in figure 9, a burn-in process was still necessary to stabilize the voltage output.† All of the boiling tests were carried out on thin film heaters that had experienced the same temperature cycling as the calibration resistance, since they were physically on the same test chip as the calibration resistor.

The final calibration curve, obtained after the cycling shown in figure 9 and extracted from branch 'B' in figure 9, is given by the following equation:

$$T = 2.106 \times 10^{-3} R_c^2 - 12.19 R_c + 17\,450, \tag{3.1}$$

where T is in kelvins and R_c (ohms) is the calibration resistance (equal to $99.91 R_{1h}$). All temperatures reported here are traced to equation (3.1).

4. Results

(*a*) *Experiments*

We measured the incipient nucleation temperature by heating TIJ thin film squares with a voltage pulse (V_{ref}) of *ca.* 5 μs duration, as in commercial printers, while the heaters were immersed in a pool of subcooled water. The parameter was V_{ref}. Figure 10 shows typical results for water. Each of the figures is for only one boiling experiment. The boiling process during the pulse heating operations was found to be quasi-static within the limits of detectability and the traces shown in figure 10 are stationary during pulses of a few hertz over many repetitions. There were no detectable changes in any of the voltage traces during these repeated pulses. The measurement accuracy itself is less than 5%, which is smaller than the size of the data symbols used in subsequent figures.

For very low voltages (and early time for high voltages), $V_{ref} < 6$ V, the average surface temperature increased in an exponential fashion that is characteristic of a lumped capacitance heater. This behaviour is expected because of the physically

† This effect is not due to changes of R_{1h}, but rather to recovery of the gold traces leading to the heater element as defects are rearranged by heating. It was eliminated by treating each test element before an experiment by applying a V_{ref} between 19 and 22 V in 1 μs pulses at a frequency of 100 Hz for 1–2 min. The bridge was then rebalanced after this (burn-in) process.

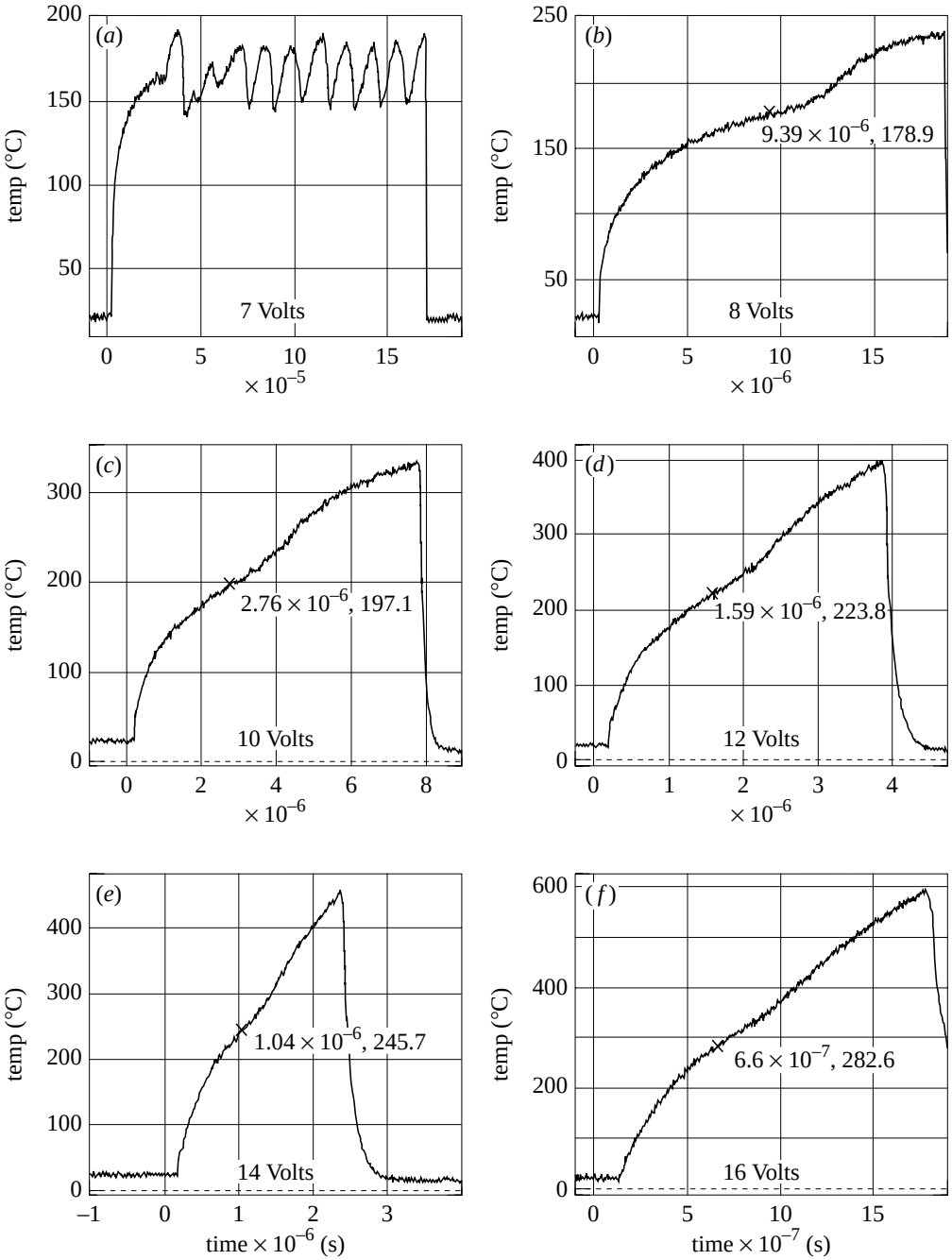

Figure 10. Measured variation of average TIJ surface temperature with input voltage, V_{ref}, indicated at the top of each figure. Temperature oscillations for $V_{\mathrm{ref}} = 7$ V indicate a cyclic bubble growth quenching process. Remainder show inflection points for various input voltages (powers). '×' in each figure indicates the nucleation temperature defined by the first inflection point, $\mathrm{d}^2T/\mathrm{d}t^2 = 0$.

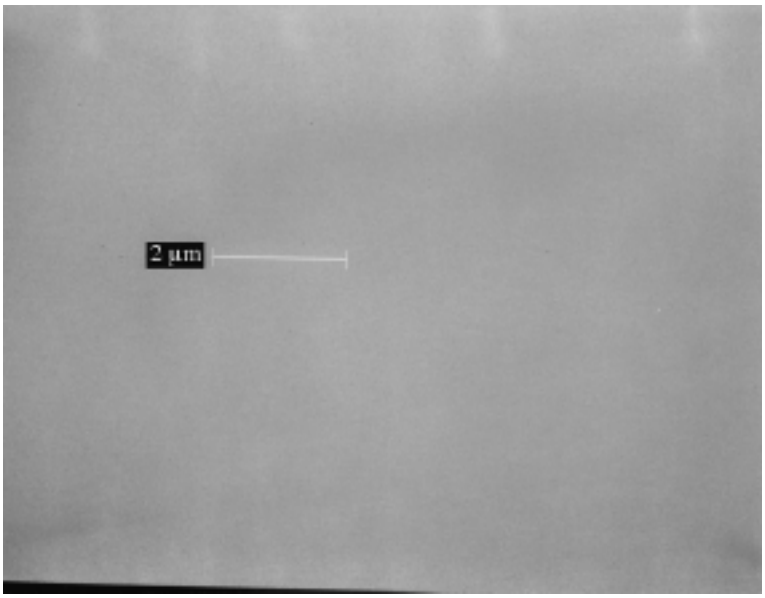

Figure 11. SEM of a portion of a TIJ thin film heater. Bar indicates 2 µm.

small TIJ resistor dimensions. For $V_{\mathrm{ref}} > 7$ V, the surface temperature increased in an exponential manner over the first 3 µs of the voltage pulse and thereafter oscillated, as shown in figure 10*a*. At higher V_{ref} values, oscillations were not observed even though the nucleation temperature was still well below the predicted homogeneous nucleation limit, as well as prior measurements for water (e.g. Avedisian 1985). We speculate below the reasons for this oscillatory temperature history at low superheat and the absence of it at high superheats.

The oscillations at low surface temperatures are due to heterogeneous nucleation of vapour bubbles forming at one or more nucleation sites. The bubble(s) go through a cyclic growth and collapse process. Because the water is subcooled, a growing bubble will encounter subcooled water on its upper perimeter and condensation will occur and collapse the bubble. During collapse, cold liquid is drawn to the surface, which lowers the surface temperature. Repeating this process oscillates the surface temperature. This collapse and quenching process has to extend over a large enough portion of the thin film heater to register a measurable surface temperature change. It can occur by either one bubble growing to cover the entire thin film heater, or by many smaller bubbles nucleating in unison at sites distributed over the surface and coalescing to blanket the surface during heat input to the liquid.

To determine if there are surface imperfections that could pass for nucleation sites on a TIJ heater, we examined the surface structure of an individual heater element by scanning electron micrography (SEM) in order to count the number of surface cavities that are present, realizing that only a fraction of these cavities would be active at any one time (Wang & Dhir 1993). Figure 11 shows an SEM, at a magnification of 10 000 times, of a portion of a Ta–Al thin film heater, and figure 6 is a photomicrograph of an entire heater. The bar in figure 11 indicates 2 µm, and roughnesses as small as 0.1 µm could be detected if present. No obvious features this small (or larger) are visible in figure 11 from the SEM pictures. Additional capabilities to detect

smaller surface features, such as by using an atomic force microscope, have revealed surface roughnesses as small as 40 Å on thin film materials (Lin 1998), or about 1000 times smaller than what could be revealed from an SEM scan like that shown in figure 11. From these facts we conclude that the nucleation site density is very low on the TIJ surfaces examined, leading to nucleation of probably no more than one or a few bubbles per individual square thin film heater. If this assessment is correct, the oscillatory temperature variation shown in figure 10 is most likely due to the aforementioned cyclic growth–collapse process of bubbles nucleating at these few sites.

At higher input voltages (and powers), temperature oscillations are not observed. Instead, the idealized form in figure 2 is realized, but the inflection point temperatures are still well below the homogeneous nucleation temperature. We conjecture that it is lateral growth but with no collapse of a few bubbles during the period of heat input that is responsible for the temperature variation. Increasing the heat transfer rate increases the bubble growth rate. If the growth phase is fast enough, rapid vapour blanketing of the surface by lateral growth can produce an inflection point in the evolution of temperature. Though it is possible that many bubbles will blanket the heater with vapour in this process, as noted above we could not detect any obvious surface features that would support the idea of multiple bubbles forming at the surface.

We took the incipient nucleation temperature to correspond to the temperature where

$$\frac{\mathrm{d}^2T}{\mathrm{d}t^2} = 0 \tag{4.1}$$

in the $T - t$ variation first occurs. This definition of nucleation is appropriate to the physics of the surface boiling process. As soon as a vapour bubble appears at the surface, the surface will start to overheat due to the presence of the vapour. The inflection point was found by curve-fitting $T - t$ variations such as shown in figure 10*b–f*, using a finite-difference method to compute the second derivative and then determining where it vanishes. The accuracy of $\mathrm{d}^2T/\mathrm{d}t^2$ depends in part on the number of data used in computing the derivatives and on the sharpness of the kink. We found that the second derivative converged when 50 adjacent temperature measurements equally divided across the inflection point were used in computing it for a given temperature trace. With this approach, our *highest* measured nucleation temperature for water was 556 K.

Figure 12 shows the variation of nucleation temperature with heating rate. As noted previously, the size of the data symbol is larger than the uncertainty of measured nucleation temperature. The nucleation temperature increases with heating rate and approaches a maximum value of 560 K, which is the extrapolation of the trend line in figure 12. The line drawn in figure 12 is meant to enhance the trend of the nucleation temperature with heating rate. A limit appears to be approached in which the nucleation temperature is independent of heating rate. In the next section we further discuss the implications of this hypothesis as it relates to homogeneous nucleation.

At the highest nucleation temperature we measured for water, the heating rate (figure 12) was about 0.25×10^9 °C s^{-1}. This heating rate is higher than the 0.093×10^9 °C s^{-1} value reported by Iida *et al.* (1994) for pulse heating water using a thin

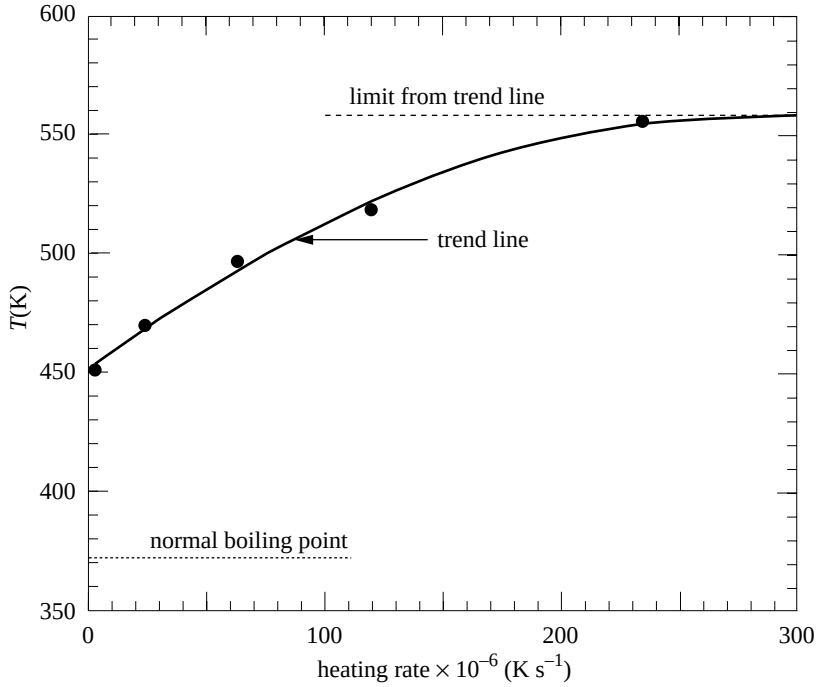

Figure 12. Variation of nucleation temperature ('×' in figure 10) with heating rate. Trend line shows an asymptote of about 560 K.

platinum film heater 0.10 mm wide and 0.25 mm long, but it is below the capabilities of high-energy laser pulse heating of liquids (Yavas *et al*. 1993). Figure 13 shows the variation of incipient nucleation temperature with input power to the thin film heaters. The power was calculated from the measured R_{1h} and V_{ref} (using equation (2.10)). As noted in § 2 *b*, approximately two-thirds of power into a TIJ heater enters the water.

(*b*) *Analysis*

To better understand the physics of the bubble nucleation process, we compare the present measurements of incipient nucleation temperature based on the inflection point in figure 10*b*–*f* with results from nucleation theory. Since the liquid is in contact with a solid surface in our experiments, a more general form of the expression for nucleation temperature includes the effect of contact angle (still assuming bubble formation by density fluctuations in the liquid (e.g. Avedisian 1998),

$$T = \frac{\Delta\Omega^*}{K}\left(\ln\frac{CN_0^{-1/3}(\xi/\Phi^{1/2})}{J_s}\right)^{-1}, \tag{4.2}$$

where $\Delta\Omega^*$ is the energy of forming a bubble in metastable equilibrium and the exponent '1/3' of N_0 accounts for the surface density of molecules (Apfel 1970). C in equation (4.2) accounts for the growth and decay process of a spherical bubble ($\theta = 0$). For a bubble that is a segment of a sphere, the factors Φ and ξ account for the volume and surface area truncation, respectively, of the bubble due to the contact

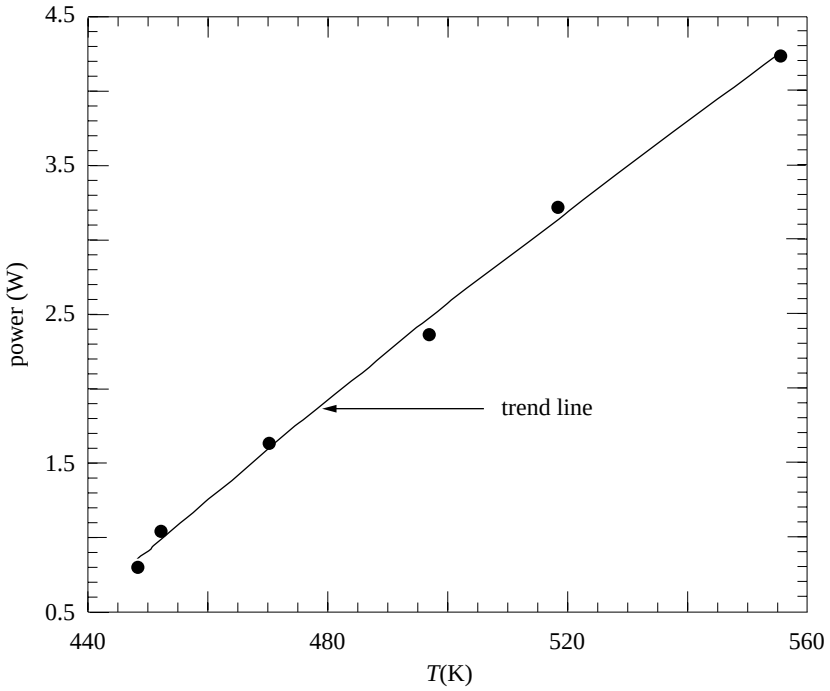

Figure 13. Variation of incipient nucleation temperature with total heat flux into a single TIJ heater.

angle (e.g. Skripov 1974; Van Stralen & Cole 1979; Debenedetti 1996; Avedisian 1998),

$$\xi = \tfrac{1}{2}(1 + \cos\theta) \tag{4.3}$$

and

$$\Phi = \tfrac{1}{4}[1 + \cos\theta]^2[2 - \cos\theta]. \tag{4.4}$$

Φ is also the ratio of the energy of forming a bubble with a truncated spherical shape to the energy of forming a spherical bubble ($\theta = 0$), $\Delta\Omega_0^*$,

$$\Delta\Omega^* = \Phi \cdot \Delta\Omega_0^*. \tag{4.5}$$

Unfortunately, we do not have contact-angle data for water on the microscale of the TIJ Ta–Al materials, and the many water–solid combinations summarized in the compilation of Adamson & Gast (1997) do not include water on the specific Ta–Al material of ink-jet printers. Notwithstanding the lack of contact-angle data for the case of interest to our study, general trends can be drawn for water–metallic surfaces that could be applicable to water on Ta–Al ink-jet materials. For example, the contact angle tends to be less than 100° for water on metals. In what follows, we will use the above results from homogeneous nucleation theory to predict the contact-angle dependence of the nucleation temperature, and then determine if the range of contact angles is plausible over which predicted and measured nucleation temperatures would agree.

In equation (4.2), J_s ($m^{-2}\,s^{-1}$) is the surface nucleation rate commensurate with the experimental conditions. It must be known before equation (4.2) can be solved (iteratively) for temperature. Avedisian (1985) shows that

$$J_s \approx \frac{1}{A'}\left|\frac{d[\Delta\Omega^*/KT]}{dT}\right|\dot{T}, \tag{4.6}$$

where $\dot{T}$ ($= dT/dt$) is the measured heating rate (upon which temperature depends, as from figure 10) and the derivative is evaluated from the variation of $\Delta\Omega^*$ with temperature (see below) and A' is the heater surface area.

It is common to use the 'classical' analysis for evaluating C, which assumes single molecule interactions with the bubble nucleus even if the energy of forming the metastable nucleus, $\Delta\Omega^*$, is evaluated from non-classical ideas of homogeneous nucleation (e.g. Oxtoby & Evans 1988). The expression for C that results from considering this classical nucleation process is (e.g. Skripov 1974; Holden & Katz 1978; Carey 1992; Debenedetti 1996; Avedisian 1998)

$$C = \sqrt{\frac{2\sigma}{\pi m}}N_0, \tag{4.7}$$

where $N_0 \approx N_{Av}/v_l$ and N_{Av} is Avogadro's number.

Two approaches for evaluating $\Delta\Omega_0^*$ are the following†. If thermophysical properties for a fluid on the scale of a bubble as small as a critical size nucleus, which is of the order of 10 Å diameter, are assumed to be the same as bulk properties (the so-called 'capillarity' approximation), then

$$\Delta\Omega_0^* = \frac{16\pi\sigma^3}{3(P^* - P_0)^2}, \tag{4.8}$$

as originally presented by Gibbs (1928). A completely different approach is to assume that the energy required to overcome the forces holding molecules together in a nucleus is the same as the energy of forming a bubble. With this idea, Kwak & Panton (1985) show that

$$\Delta\Omega_0^* = \frac{1}{54}\frac{(z\varepsilon_m)^3}{(v_m(P - P_0))^2}, \tag{4.9}$$

where v_m is the molecular volume, ε_m is the 'area' under the intermolecular potential curve and z is the number of nearest-neighbour molecules. Kwak & Panton (1985) assume a face-centred cubic (FCC) structure and a Lennard–Jones fluid for which $z = 12$ and

$$\varepsilon_m = 4\varepsilon_0\left(1 - \left(\frac{v_m}{v_c}\right)^2\right)\left(\left(\frac{d_w}{d_m}\right)^6 - \left(\frac{d_w}{d_m}\right)^{12}\right),$$

respectively, where

$$\varepsilon_0 \approx \tfrac{3}{16}E_i\gamma/d_w^6.$$

† There are additional methods of determining the energy of forming a critical size bubble. They involve determining the density variation across the liquid–vapour interface to compute the energy of forming the metastable equilibrium bubble energy, as in the density functional theory applied to the nucleation problem by Oxtoby & Evans (1988).

E_i, γ and d_w are the ionization potential, polarizability and hard sphere (van der Waals) diameter of the fluid, respectively. All values are known for water. For an FCC molecular packing,

$$d_\mathrm{m} = \left(0.7405\frac{6}{\pi}v_\mathrm{m}\right)^{1/3}.$$

To solve equation (4.2) for temperature using equations (4.8) or (4.9) for the energy of the bubble, we need to estimate J_s.

J_s was estimated from equation (4.6) using the measured heating rate (figure 10), equation (4.8) for $\Delta\Omega_0^*$ (which we assume will be adequate as far as estimating J_s is concerned), and $\mathrm{d}[\Delta\Omega^*/KT]/\mathrm{d}T$ evaluated from equation (4.8) using the temperature dependence of property values from data listed in Keenan *et al.* (1969) and Vargaftik *et al.* (1983) for saturation pressure (P_s), liquid specific volume (v_l) and surface tension (σ). Figure 14 shows the variation of J_s with heating rate at several temperatures, where A' in equation (4.6) is the surface area of one heater. The nucleation rate varies from 10^{16} to 10^{21} m^{-2} s^{-1} over the range of heating rates and temperatures shown. Even though this range seems large, the nucleation rate appears in a logarithmic term in equation (4.2), and that dampens the effect of J_s on temperature so that J_s is, for all practical purposes, a fixed value as far as the nucleation temperature is concerned. In equation (4.2) we take a mean value of $J_\mathrm{s} \approx 10^{19}$ m^{-2} s^{-1}. Because $J_\mathrm{s} \propto \dot{T}$ (from equation (4.6)), and thus $\dot{T}$ also implicitly appears in the logarithm in equation (4.2), the measured nucleation temperature should have a weak dependence on heating rate if homogeneous nucleation is the operative mechanism of bubble formation. From figure 12, the nucleation temperature is suggested to approach a value that is almost independent of $\dot{T}$ as $\dot{T}$ increases. At lower heating rates the nucleation temperature is proportional to heating rate which is not consistent with equation (4.2) and, thus, a homogeneous nucleation mechanism.

Figure 15 shows the calculated variation of nucleation temperature (the solution to equation (4.2)) with contact angle corresponding to $J_\mathrm{s} = 10^{19}$ m^{-2} s^{-1}. In equation (4.2), the relationship between vapour pressure (P) in the bubble and P_s that arises by the finite curvature of the bubble was included (e.g. Avedisian 1986). $\theta = 0$ corresponds to a spherical bubble forming at the surface. $\theta \to 180°$ is the completely wetting limit that produces 'nucleation' at the normal boiling point which is the case of equilibrium across a 'flat' liquid–vapour interface. Results from the classical approach to computing $\Delta\Omega_0^*$ (equation (4.8)) and the analysis of Kwak & Panton (1985) (equation (4.9)) are shown.

Both equations (4.8) and (4.9) show the same general trend with contact angle: as the contact angle decreases the nucleation temperature approaches a value corresponding to a spherical bubble. For both models of $\Delta\Omega_0^*$, the nucleation temperature shows a large range of contact angles over which the nucleation temperature is not strongly dependent on contact angle. Using equation (4.8), our measured maximum nucleation temperature is within 5% of the spherical bubble limit (which corresponds to $\theta = 0°$) for contact angles in the range $0 \leqslant \theta \leqslant 140°$. When equation (4.9) is used for determining $\Delta\Omega_0^*$, the nucleation temperature is within 5% of the spherical bubble value for $0 \leqslant \theta \leqslant 115°$.

Comparing figure 15 with the data in figure 12, virtually the entire range of measured nucleation temperatures will fall within the predicted ranges shown in figure 15

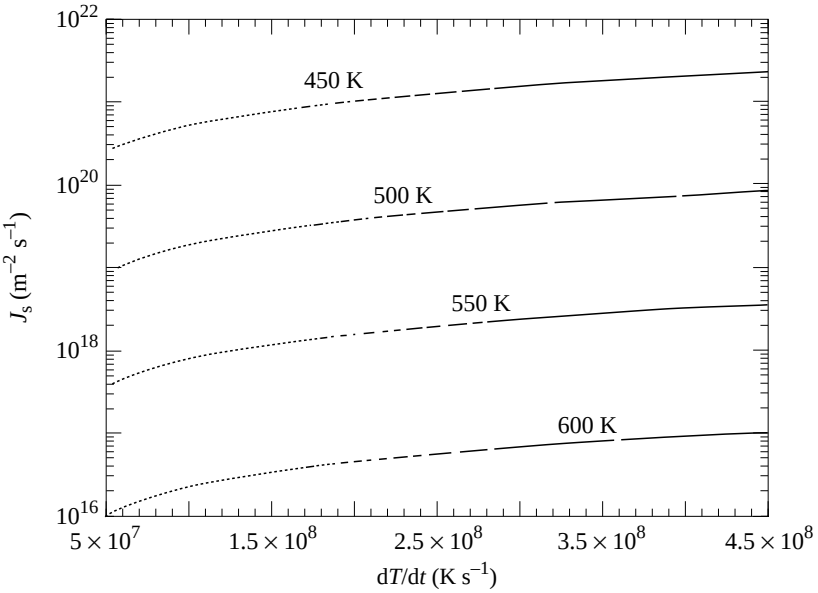

Figure 14. Estimated surface nucleation rate from equation (4.6).

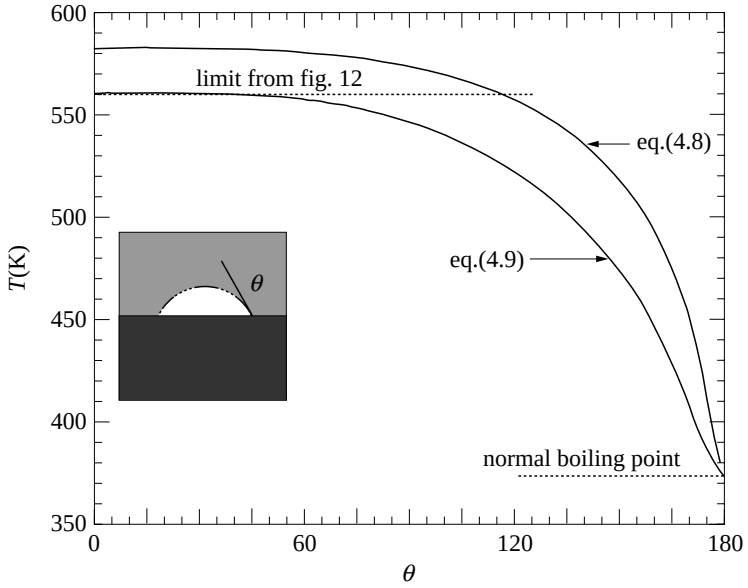

Figure 15. Predicted homogeneous nucleation temperature with contact angle for water assuming $J_s = 10^{19}$ m^{-2} s^{-1} in equation (4.2).

if the contact angle is adjusted appropriately. However, the contact angles spanned in figure 15 are *not* all relevant to the fluid–material combination we have examined. The compilation of Adamson & Gast (1997) shows that for water on many metal surfaces, the contact angle is often under 100°. On gold and glass it is listed as 'small' or '0°' and on platinum it is 40°, all at room temperature. Considering that

Table 1. *Some peak-measured nucleation temperatures for water at atmospheric pressure*

temperature (K)	heating rate ($K\ s^{-1}$)	fluid containment	characteristic dimension of heated volume (μm)	reference
552.7	0.7	droplet in immiscible liquid	200 to 500	Apfel (1972)
553	3.0	droplet in immiscible liquid	100 to 500	Blander *et al.* (1971)
556	2.5×10^8	Ta–Al plate	64.5 by 64.5	present study
563	9.0×10^6	platinum wire	25 by 10 000	Derewnicki (1985)
568	9.3×10^7	platinum plate	100 by 250	Iida *et al.* (1994)

the contact angle decreases with increasing temperature, the contact angle should be smaller at the temperatures measured in this study. Returning to figure 15, the variation of nucleation temperature with contact angle is flat for $\theta < 100°$, changing by only a few per cent for $0 < \theta < 100°$. Because the predicted nucleation temperature in figure 15 that is approached by both models for $\Delta\Omega_0^*$ as the contact angle is reduced is quite close to the upper limit approached as heating rate is increased, we conclude that our highest measured nucleation temperature, of 556 K, is due to a homogeneous nucleation mechanism. The contact-angle range that predicts this value is well within the range for many water–metal combinations. Our lower measured nucleation temperatures that correspond to the reduced heating rates in figure 12 cannot be explained by homogeneous nucleation theory because the contact angle would have to be too large according to figure 15, which is contrary to the trend for many water–metal combinations.

We compare in table 1 our peak measured nucleation temperature for water with prior published values which used various heating techniques and liquid containment. In the studies listed, water was in contact with media that included heated wires or plates, or a 'droplet' with its containment being a liquid–liquid interface. Also included in table 1 are the corresponding heating rates reported or estimated from the references. The highest nucleation temperature we measured, 556 K, is well within the range measured by Derewnicki (1985) and Iida *et al.* (1994), who used platinum wires and plates, respectively. The heating rates are comparable, differing by two orders of magnitude (which produces differences in J_s that still do not strongly affect the nucleation temperature). Furthermore, as noted previously, $\theta < 40°$ for water on platinum (Adamson & Gast 1997), which is a low enough contact angle that the predicted surface nucleation temperature should be at its maximum value, which according to figure 15 is close to these measured values.

The floating droplet methods of Apfel (1972) and Blander *et al.* (1971) produced peak nucleation temperatures for water only *ca.* 4 K lower than measured here, yet their heating rates were nine orders of magnitude lower. The much lower heating rates required to produce homogeneous nucleation within a droplet suspended in another immiscible liquid is a consequence of the fact that the droplet–host fluid interface is smooth on the molecular level while a solid–liquid interface is usually not. A solid surface invariably has a roughness that traps gas during flooding of the surface with liquid and nucleate boiling is the process of gas trapped in these pockets

emerging as bubbles from the surface. A certain time is needed for this process to occur. If the heating rate is high enough, a uniformly heated fluid in contact with a solid surface can reach the homogeneous nucleation temperature at those parts of the surface which are 'smooth' before bubbles nucleate in the 'rough' parts. This is the viewpoint for the experimental conditions examined here. On the other hand, for 'low' heating rates, the surface temperature cannot reach the homogeneous nucleation temperature before nucleate boiling from roughness features is triggered. This latter situation is commonly encountered in most boiling processes of solid–liquid contact. The intense heating associated with ink-jet printing is a special case where homogeneous nucleation at a solid surface can occur before nucleate boiling because of the high heating rates involved.

5. Summary

1. The experimental results show that homogeneous nucleation at a surface is the mechanism for bubble formation for the highest heating rate measured.
2. Measured and predicted nucleation temperatures are in qualitative agreement if an appropriate contact angle is selected.
3. The nucleation temperature increases as the heating rate increases.
4. The variation of electrical resistance with temperature of the Ta–Al thin film heaters showed unusual effects of cycling temperature in which the resistance was not stable until the heater temperature had been cycled. This effect indicates the necessity of annealing the thin film heaters before nucleation experiments are performed.
5. The electrical resistance decreases as temperature increases for the Ta–Al heaters studied. This trend is opposite to either Al or Ta alone.
6. The maximum heating rate measured was $0.25 \times 10^9\ \mathrm{K\,s^{-1}}$.

This research could not have been carried out without the help of a number of individuals. Ross Allen and Brian Canfield of Hewlett–Packard Corporation (HP) were instrumental in the early stages to arrange for support and advice. Also from HP we thank Dave Thomas, Paul Harmon, Dave Chrisman, Jay Dickinson, Dave Pinkernell, Alfred Pan and John Meyers for valuable input, resources and arranging for fabrication of the test chips studied. WSB especially wishes to thank HP for a VPR fellowship. Dr Sanjeev Chandra of the University of Toronto worked on the circuit design in the early phases of this study while he was at Cornell. Mr Jeffrey Barr of Hewlett–Packard and Mr Steven Sax of the Naval Research Laboratory carried out initial calibration studies also while students at Cornell. This paper is the evolutionary development of these efforts. C.T.A. thanks Ms Aleksandra P. Chojnacka for insights on ink-jet materials and help with SEM and photomicrography. Comments from an anonymous referee were also helpful.

References

Adamson, A. W. & Gast, A. P. 1997 *Physical chemistry of surfaces*, 6th edn, pp. 365–366. Wiley.

Allen, R. R., Meyer, J. D. & Knight, W. R. 1985 Thermodynamics and hydrodynamics of thermal ink jets. *Hewlett Packard J.* **36**, 21–27.

Apfel, R. E. 1970 Vapor cavity formation in liquids. Technical Memorandum no. 62, Acoustics Research Laboratory, Harvard University.

Apfel, R. E. 1972 Water superheated to 279.5 °C. *Nat. Phys. Sci.* **238**, 63–64.

Avedisian, C. T. 1985 The homogeneous nucleation limits of liquids. *J. Phys. Chem. Ref. Data* **14**, 695–720.

Avedisian, C. T. 1986 Bubble growth within superheated liquid droplets. In *Encyclopedia of fluid mechanics*, vol. 3, ch. 8, pp. 130–190. Houston, TX: Gulf Publishing Co.

Avedisian, C. T. 1998 Modeling homogeneous bubble nucleation in liquids. In *Modeling of engineering heat transfer phenomena*, ch. 11. London: Computational Mechanics.

Blander, M., Hengstenberg, D. & Katz, J. L. 1971 Bubble nucleation in *n*-pentane, *n*-hexane, *n*-pentane + hexadecane mixtures, and water. *J. Phys. Chem.* **75**, 3613–3619.

Carey, V. P. 1992 *Liquid–vapor phase-change phenomena*. Washington, DC: Hemisphere.

Debenedetti, P. G. 1996 *Metastable liquids*, pp. 179, 218–222. Princeton University Press.

Derewnicki, K. P. 1985 Experimental studies of heat transfer and vapour formation in fast transient boiling. *Int. J. Heat Mass. Transf.* **28**, 2085–2092.

Gibbs, J. W. 1928 *The collected works of J. Willard Gibbs*, vol. 1. London: Longmans Green.

Holden, B. C. & Katz, J. L. 1978 The homogeneous nucleation of bubbles in superheated binary liquid mixtures. *AIChE J.* **24**, 242–260.

Iida, Y., Okuyama, K. & Sakurai, K. 1993 Peculiar bubble generation on a film heater submerged in ethyl alcohol and imposed a high heating rate over 10^7 K s^{-1}. *Int. J. Heat Mass Transf.* **36**, 2699–2701.

Iida, Y., Okuyama, K. & Sakurai, K. 1994 Boiling nucleation on a very small film heater subjected to extremely rapid heating. *Int. J. Heat Mass Transf.* **37**, 2771–2780.

Incropera, F. P. & DeWitt, D. P. 1996 *Fundamentals of heat and mass transfer*, 4th edn, pp. 239, 829, 832, 846. Wiley.

Keenan, J. H., Keyes, F. G., Hill, P. G. & Moore, J. G. 1969 *Steam tables*. Wiley.

Kwak, H. Y. & Panton, R. L. 1985 Tensile strength of simple liquids predicted by a model of molecular interactions. *J. Phys.* D **18**, 647–659.

Lee, F. C. & Tirumala, M. 1988 An investigation of bubble dynamics in thermal ink jet. Report RJ 6292 (61689), IBM Research Division, Yorktown Heights, June 16.

Lide, D. R. 1992 *Handbook of chemistry and physics*, 72nd edn, pp. 12–34. Boston, MA: CRC Press.

Lin, L. 1998 Microscale thermal bubble formation: thermophysical phenomena and applications. *Microscale Thermophysical Engng* **2**, 71–85.

Nielsen, N. J. 1985 History of ThinkJet printhead development. *Hewlett Packard J.* **36**, 4–10.

Okuyama, K. & Iida, Y. 1990 Transient boiling heat transfer characteristics of nitrogen (bubble behavior and heat transfer rater at stepwise heat generation). *Int. J. Heat Mass. Transf.* **33**, 2065–2071.

Okuyama, K., Kozawa, Y., Inoue, A. & Aoki, S. 1988 Transient boiling heat transfer characteristics of R113 at large stepwise power generation. *Int. J. Heat Mass. Transf.* **31**, 2161–2174.

Olive, G., Moore, J. O., Tirumala, M. & Eldridge, J. M. 1988 Experimental study of temperature transients in thin film thermal ink jet heaters. Report RJ 6450 (62923), IBM Research Division, Yorktown Heights, June 28.

Osborne, B. 1996 Master of Engineering Report. Sibley School of Mechanical and Aerospace Engineering, Cornell University, August.

Oxtoby, D. W. & Evans, R. 1988 Nonclassical nucleation theory for the gas–liquid transition. *J. Chem. Phys.* **89**, 7521–7530.

Poppel, J. 1989 Measurement of temperature transients at the heater of a bubble jet by detection of the nucleation. *SID 89 Digest*, 176–179.

Skripov, V. P. 1974 *Metastable liquids*. Wiley.

Van Stralen, S. J. D. & Cole, R. 1979 *Boiling nucleation*, vol. 1. McGraw-Hill.

Vargaftik, N. B., Volkov, B. N. & Voljak, L. D 1983 International tables of the surface tension of water. *J. Phys. Chem. Ref. Data* **12**, 817–820.

Wang, C. H. & Dhir, V. K. 1993 On the gas entrapment and nucleation site density during pool boiling of saturated water. *J. Heat Transf.* **115**, 670–679.

Yavas, O., Leiderer, P., Park, H. K., Grigoroupoulos, C. P., Poon, C. C., Leung, W. P., Do, N. & Tam, A. C. 1993 Optical reflectance and scattering studies on nucleation and growth of bubbles at a liquid–solid interface induced by pulsed laser heating. *Phys. Rev. Lett.* **70**, 1830–1833.